

Shaping Nanoparticles with Hydrophilic Compositions and Hydrophobic Properties as Nanocarriers for Antibiotic Delivery

Yusilawati Ahmad Nor,[†] Yuting Niu,[†] Surajit Karmakar,[†] Liang Zhou,[†] Chun Xu,[†] Jun Zhang,[†] Hongwei Zhang,[‡] Meihua Yu,[†] Donna Mahony,[‡] Neena Mitter,[‡] Matthew A. Cooper,[§] and Chengzhong Yu^{*,†}

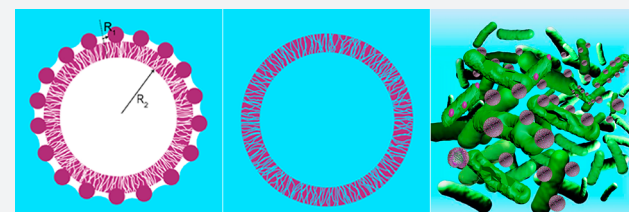
[†]Australian Institute for Bioengineering and Nanotechnology, The University of Queensland, Brisbane, Queensland 4072, Australia

[‡]Queensland Alliance for Agriculture and Food Innovation, The University of Queensland, Brisbane, Queensland 4072, Australia

[§]Institute for Molecular Bioscience, The University of Queensland, Brisbane, Queensland 4072, Australia

Supporting Information

ABSTRACT: Inspired by the lotus effect in nature, surface roughness engineering has led to novel materials and applications in many fields. Despite the rapid progress in superhydrophobic and superoleophobic materials, this concept of Mother Nature's choice is yet to be applied in the design of advanced nanocarriers for drug delivery. Pioneering work has emerged in the development of nanoparticles with rough surfaces for gene delivery; however, the preparation of nanoparticles with hydrophilic compositions but with enhanced hydrophobic property at the nanoscale level employing surface topology engineering remains a challenge. Herein we report for the first time the unique properties of mesoporous hollow silica (MHS) nanospheres with controlled surface roughness. Compared to MHS with a smooth surface, rough mesoporous hollow silica (RMHS) nanoparticles with the same hydrophilic composition show unusual hydrophobicity, leading to higher adsorption of a range of hydrophobic molecules and controlled release of hydrophilic molecules. RMHS loaded with vancomycin exhibits an enhanced antibacterial effect. Our strategy provides a new pathway in the design of novel nanocarriers for diverse bioapplications.



In biological systems, hydrophobic interaction is reported to be the strongest of all long-range noncovalent interactions, which is beneficial for adsorption of biomolecules,^{1–3} improving interaction/adhesion with cellular membranes,^{2,4} increasing the uptake of nanoparticles for cellular delivery,² as well as tailoring the release rate of drugs.⁵ To generate nanoparticles with hydrophobic properties, the choices of hydrophobic composition or functionalization are among the convenient approaches. Hydrophobic materials such as carbon nanotubes (CNTs) have shown great promise as nanovehicles for drug delivery; however, one of the main concerns is the fact that CNTs could be hazardous to environment and human health which need further surface functionalization to reduce their intrinsic toxicity.⁶ Hydrophobic moieties such as alkanethiols and alkyl chains have been modified onto the surfaces of various nanoparticles including gold^{7,8} and silica^{9,10} to enhance the loading of hydrophobic drugs/protein^{7,9,10} and improve cellular delivery performance.^{9,10} However, chemically grafted hydrophobic groups tended to cause unwanted toxicity¹¹ and pore blocking of mesoporous nanocarriers.^{10,12} It is a challenge to design a safe and efficient nanocarrier system employing an alternative approach.

Surface topographical modification is a nature-inspired approach to adjust the hydrophilic/hydrophobic property and wetting behavior of materials. It has been well-known that superhydrophobic surfaces can be created by having a micro- or

nanotextured surface made of hydrophobic materials which have versatile real life applications.^{13–19} In parallel to the progress made in designing superhydrophobic materials, characterization of their wetting properties has been addressed with experiments, theory, and computer simulations.¹⁸ Recent studies have demonstrated that it is possible to fabricate a hydrophobic surface from hydrophilic materials through either surface porosity²⁰ or surface roughness engineering.^{21,22} However, previous studies mainly focused on large flat surfaces; nanoparticles with hydrophilic compositions and hydrophobic properties through surface roughness control have not been reported.

Herein we report the unusual properties exhibited by rough mesoporous hollow silica (RMHS) nanoparticles with a hydrophilic composition. As shown in Figure 1, this approach relies on surface roughness engineering by adding silica shell particles with smaller sizes (~13 or 30 nm in diameter) onto MHS with relatively larger sizes (~200 or 400 nm). The surface roughening creates the voids (the space between small shell spheres with a radius of R1) on the outer surface for air entrapment. The air pocket is significantly enlarged in our design because the internal spherical cavity with a much larger radius of R2 than R1 is connected with the air through the

Received: May 22, 2015

Published: September 9, 2015

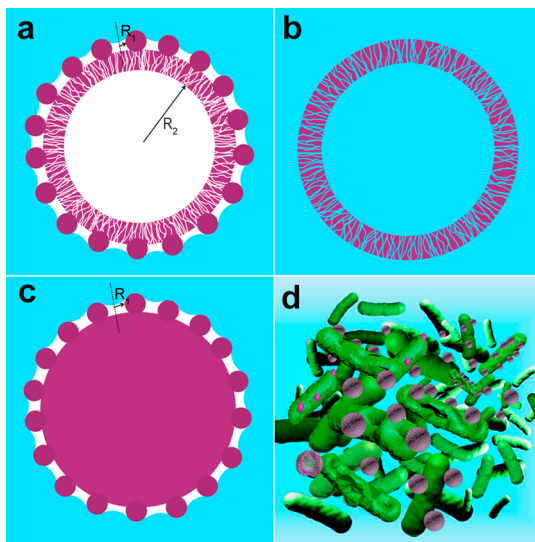


Figure 1. Schematic diagram of the hydrophobic nature of the nanoparticles created by surface engineering. (a) The void spaces (the spaces between small shell spheres with a radius of R_1) on the surface of RMHS are generated for air (white color) entrapment. Additional internal spherical cavity with a radius of R_2 connected with the air through the mesopores in the shell in RMHS (pink color) provides an energy barrier which delays the wetting state. (b) MHS (pink color) with silanol ($\text{Si}-\text{OH}$) composition tends to adsorb water molecules (blue color). (c) The absence of an internal cavity reduces the hydrophobic property and has lower loading capacity. (d) The delivery of antibiotic to bacteria (green color) culture.

mesopores channel in the silica shell. The repulsion of the trapped air (white color in Figure 1a) in the void spaces toward water molecules (blue color in Figure 1a) provides the energy barrier against the wetting process because the hydroxyl groups in silica (SiO_2 , pink color Figure 1a) tend to adsorb water molecules as in the case of mesoporous hollow silica (MHS, Figure 1b).²³ Compared to rough solid Stöber (RSS) silica nanoparticles (Figure 1c), RMHS provide more space to trap the air, leading to a higher energy barrier during the wetting process and thus more distinguished hydrophobicity. The nature of hydrophilic composition of RMHS provides a high loading capacity of the “last resort” antibiotic vancomycin (VAN), whereas the hydrophobic behavior influenced by surface roughness facilitates the delayed release of VAN and improved interaction with bacteria, resulting in enhanced antibacterial efficacy (Figure 1d), compared to free VAN and MHS-VAN.

RESULTS AND DISCUSSION

MHS nanoparticles were synthesized using a surfactant-directing alkaline etching strategy.²⁴ RMHS was prepared by mixing positively charged MHS after amino group functionalization with negatively charged Stöber silica nanoparticles (~ 40 nm in diameter) followed by calcination at 550°C for 6 h in air. Scanning electron microscope (SEM) and high-resolution transmittance electron microscopy (HRTEM) images show that RMHS of 450 nm in average size have been successfully prepared with a uniform spherical morphology (Figure 2a,c). The surfaces of RMHS are homogeneously decorated with ~ 40 nm silica nanospheres, indicating the successful attachment of silica nanospheres to the surface of MHS. The distance between two neighboring silica nanospheres is measured at around 30

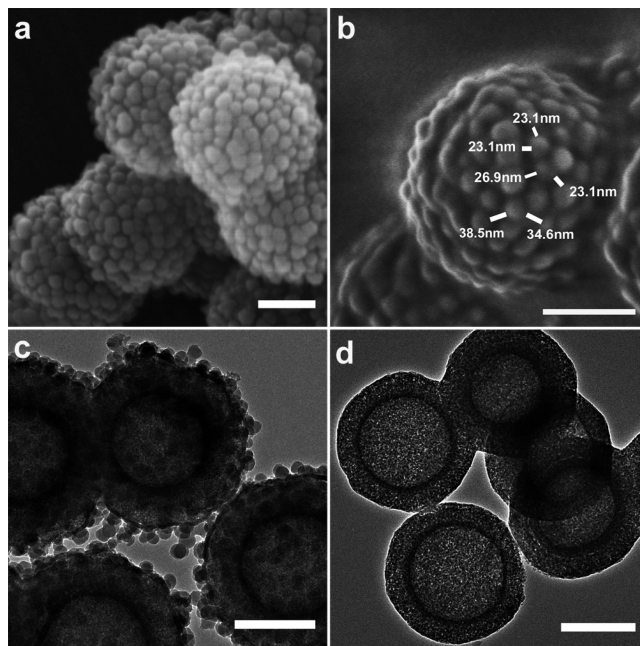


Figure 2. Surface morphology of RHMS and MHS nanoparticles. (a) SEM image of RMHS, (b) high-resolution scanning electron microscope (HRSEM) image of RMHS showing the distance between neighboring shell silica nanospheres that responsible for air entrapment, (c) and (d) HRTEM images of RMHS and MHS respectively. Scale bar = 200 nm.

nm (Figure 2b), and the gap between them provides space for the air entrapment. In contrast, MHS (Figure 2d) has an average particle size of 350 nm with a relatively smooth surface. HRTEM images (Figure 2c,d) clearly indicate the hollow core@porous shell structure of RMHS and MHS. The hollow core is ~ 230 nm in diameter and the porous shell is about 60 nm in thickness. SEM and TEM images in Figure S1 show the hollow core of the nanoparticles with uniform morphology for both MHS (Figure S1a–c) and RMHS (Figure S1d). The hydrodynamic diameter of MHS and RMHS was further measured by dynamic light scattering (DLS), which shows a number mean size ($D_{1,0}$) of 396 ± 63 nm for MHS and 459 ± 55 nm for RMHS (Figure S2), consistent with both SEM and TEM results.

Both MHS and RMHS exhibited typical type-IV isotherms with an H2-type hysteresis loop, indicating the existence of well-defined mesopores (Figure S3a). The pore size distributions calculated from the adsorption branches using the Barrett–Joyner–Halenda (BJH) method showed that both samples have uniform mesopores centered at 3.5 nm (Figure S3b). RMHS has a relatively lower surface area compared to MHS (342 vs $427 \text{ m}^2 \text{ g}^{-1}$) because the shell particles are solid. The higher pore volume of RMHS (0.46 vs $0.31 \text{ cm}^3 \text{ g}^{-1}$ of MHS) is mainly attributed to the interparticle packing voids as reflected by the capillary condensation step, which occurred at relative pressure (P/P_0) higher than 0.90 (Figure S3a and Table S1). The mesopore volume (V_{meso}) is calculated to be 0.34 and $0.35 \text{ cm}^3 \text{ g}^{-1}$ for MHS and RMHS, respectively. Surface charge measurement by ζ -potential showed that both RMHS and MHS were negatively charged to a similar degree both in water and PBS buffer in pH 7.4 (Table S1). Both samples have pure silica in composition, as confirmed by Fourier transform infrared spectroscopy (FTIR) (Figure S4), showing characteristic peaks for physisorbed water ($-\text{OH}$) at 1620 cm^{-1} , silanol

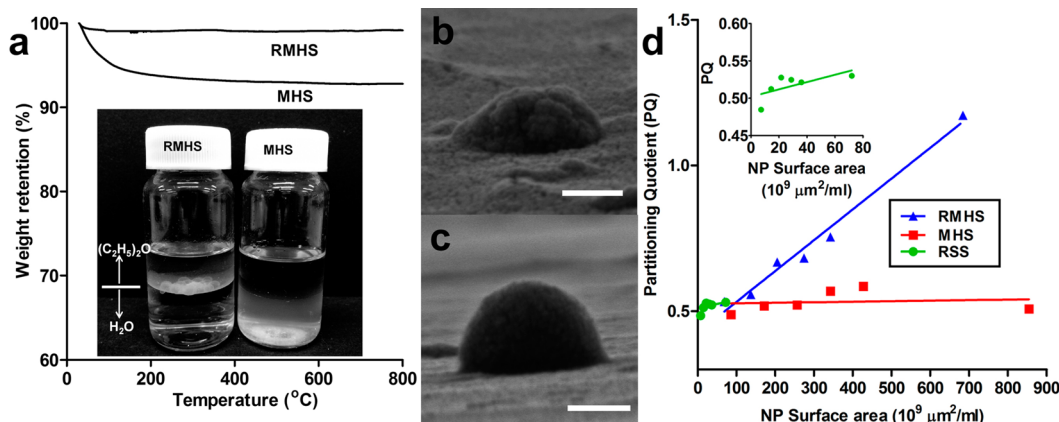


Figure 3. Hydrophobicity of nanoparticles. (a) TGA profiles of RMHS and MHS measuring water content adsorb by the particles at 100–200 °C. Inset showing the dispersion behavior of RMHS and MHS in diethyl ether/water layer after shaking. The HRSEM of (b) RMHS and (c) MHS on PDMS layer for measuring individual contact angle by the gel trapping method (GTT). Scale bar = 200 nm and (d) hydrophobicity measurements via rose bengal (RB) partitioning.

group (Si—OH) at 790 cm^{−1}, as well as siloxane group (Si—O—Si) at 1062 and 449 cm^{−1}.

The hydrophobicity of the nanoparticles was characterized by the dispersion of MHS and RMHS in diethyl ether-water two phase systems. As seen from the inset of Figure 3a, RMHS thermodynamically favored the bottom of the diethyl ether layer (a hydrophobic solvent) with shaking while MHS directly disperses in the water layer (a hydrophilic solvent) when added to the system. RSS showing similar behavior as RMHS in the water/diethyl ether layer as shown in Figure S5b. This occurred due to the competition between the affinity of Si—OH toward water molecules and the repulsion of the trapped air in void spaces toward both oil and water molecules (as described in Figure 1). Thermal gravimetric analysis (TGA) profiles presented a small weight loss of 0.9% below 200 °C for RMHS but 7.2% for MHS, which can be attributed to the evaporation of moisture. The TGA results indicate that the introduction of surface roughness makes RMHS more hydrophobic, and thus, it absorbs less moisture from the atmosphere compared to MHS.

The hydrophobicity of a film surface can be easily quantified by the contact angle measurement. However, this technique does not readily apply for nanoparticles because in general their diameters are much smaller compared to that of a liquid droplet. To provide a quantitative comparison of the hydrophobicity between RMHS and MHS, a gel trapping technique (GTT) (see Supporting Information and Figure S6) was employed. The GTT method to measure the hydrophobicity of nanoparticles was developed by Paunov and co-workers^{25–27} followed by SEM measurement. Arnaudov et al. later successfully measured the contact angle of nanoparticles with radii as small as 37 nm by the GTT method followed by AFM,²⁸ suggesting that the GTT method can be applied to measure the contact angle of nanoparticles with variable sizes. The HRSEM images of the RMHS (Figure 3b) and MHS (Figure 3c) on the PDMS layer obtained with GTT were picked up from the decane–water interfaces. Individual RMHS were mostly embedded in the PDMS while MHS is clearly visible on the PDMS surface showing a contact angle value of 107.5° ± 10° (*n* = 5) for RMHS and 72.5° ± 5° (*n* = 5) for MHS. The contact angle value of RMHS is however lower than that obtained for the octadecyltrimethoxysilane (C18) modified silica (~136°) of an average diameter of 2.15 μm measured

with the same method in a previous report.²⁵ These results agreed with the scheme in Figure 1 and with the oil/water results in Figure 3a.

A dye (rose bengal, RB) adsorption method was also employed to quantitatively determine the relative hydrophobicity of nanoparticles.^{29,30} A plot of partitioning quotient (PQ) versus nanoparticle surface area per milliliter was constructed for RMHS, MHS, and RSS, as provided in Figure 3d, and the value was given in Table S1. The slope of this plot is proportional to the relative hydrophobicity of nanoparticles. Compared to RSS with the slope of 0.000675 × 10^{−9} ml μm^{−2}, RMHS yielded a higher slope value of 0.00106 × 10^{−9} ml μm^{−2}, indicating higher hydrophobicity of RMHS compared to RSS. MHS on the other hand showed the lowest slope with no significant value suggesting a hydrophilic nature of silica. Both qualitative and quantitative measurements (Figure 3, Figure S5b) are in agreement with the theory proposed in Figure 1.

We further compared the adsorption behavior of three different proteins including RNase A (RNASE), insulin (INS), and lysozyme (LYS), a hydrophobic dye, disperse red 1 (DR1), and a hydrophobic drug, griseofulvin (GRIS), on the nanoparticles. It has been reported elsewhere that a surface after hydrophobic modification has increased adsorption capacity toward RNASE,^{9,10} INS,³¹ and LYS.³² As shown in Figure 4a, a higher loading capacity was achieved exclusively for five sorbates (see quantitative comparison in Table S2) by RMHS than MHS. Compared to MHS, a faster adsorption rate of DR1 (Figure 4b) and LYS (Figure S7a) was also observed when comparing RMHS to MHS. All the samples in Figure 4a,b have been pretreated by sonication to disperse the particles prior to the addition of drug or protein. LYS concentration in the absence of particles before and after rotation and centrifugation was also measured as a control. No significant difference between initial and final concentrations of the LYS solution was observed (data not shown), indicating no precipitation of LYS occurred during the process.

Porous nanocarriers with high surface area and pore volumes are beneficial for high loading capacity of cargo molecules.³³ However, when the nanocarriers are dispersed in aqueous solution for adsorption, the pore volume generated by the interparticle packing voids during the nitrogen adsorption–desorption measurements should not contribute to the loading of molecules. Compared to MHS, RMHS has a lower surface

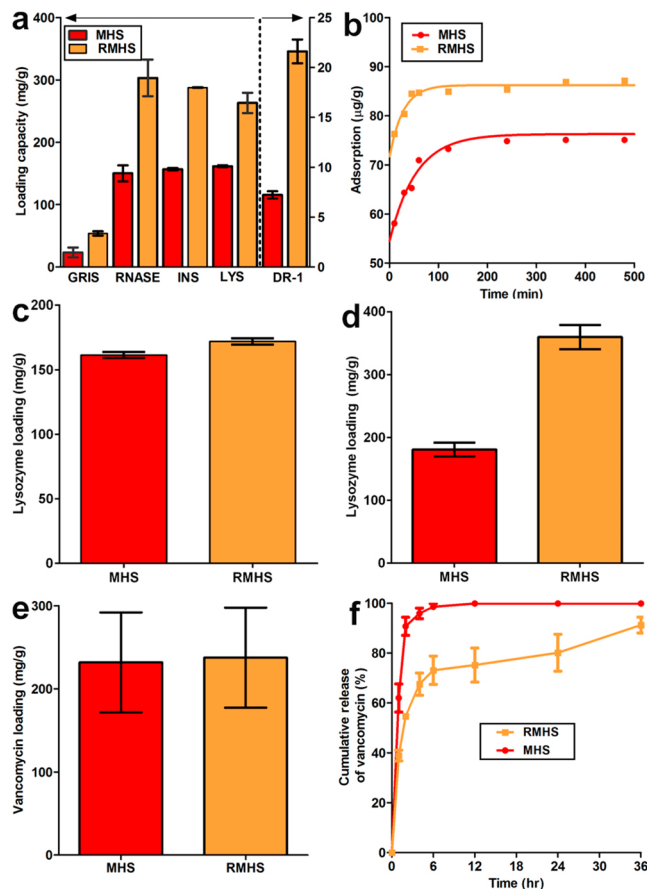


Figure 4. Uptake and release behavior of the nanoparticles toward different molecules. (a) Loading capacity of MHS and RMHS on drug and different proteins, (b) uptake rate of DR1, (c) loading of LYS in vacuum environment, (d) loading of LYS without pretreatment by sonication, (e) loading of VAN, and (f) the cumulative release profile of VAN from nanoparticles. The particles (except in d) were pretreated with sonication to disperse the particles before adding the proteins or drugs for loading. The error bars reflect the standard deviation of the measurements.

area and comparable mesopore volume (Table S1), suggesting that neither the surface area nor the mesopore volume is responsible for the higher loading capacity of RMHS over MHS for the five sorbates (Table S2). It is hypothesized that the enhanced hydrophobicity of nanoparticles with rough surfaces favors higher and faster loading of cargo molecules under study.

To further support our hypothesis and understand the role of air which induced RMHS hydrophobicity, the adsorption capacity of RMHS toward LYS was conducted in a vacuum environment where air bubbles are removed from the suspension. The adsorption amount of the LYS on RMHS was reduced by 37.3% (from 263.1 mg g⁻¹ to 172.1 mg g⁻¹), comparable with the adsorption capacity of MHS (161.5 mg g⁻¹, Figure 4c). Similarly, lower loading capacity of LYS was achieved for RMHS pretreated by shaking and stirring for 36 h to remove the air with 7.6% (from 263.1 to 243.1 mg g⁻¹) and 30% (from 263.1 to 184.1 mg g⁻¹) reduction, respectively. On the other hand, an additional experiment was conducted by eliminating the presonication process to retain most of the air trapped by the nanoparticles. Higher loading of LYS was achieved by RMHS without sonication with 37.4% increment (from 263.1 mg g⁻¹ to 361.4 mg g⁻¹, Figure 4d) compared to the adsorption using RMHS subject to presonication steps in

Figure 4a. The above observations further support our hypothesis that the loading of LYS is dependent on the amount of air entrapped. Air as the hydrophobic solvent on the RMHS structure subsequently improves the adsorption for hydrophobic molecules such as LYS. Methods that can remove or partially remove air (such as vacuum, sonication, shaking, and vigorous stirring treatment) will decrease the LYS loading capacity.

The loading capacity of RSS toward LYS was also measured (Figure S5c, 25.9 mg g⁻¹). Compared to that of RMHS (263.1 mg g⁻¹), the much lower LYS loading amount of RSS can be attributed to its solid nature. Surface roughness has no influence on the loading capacity of a hydrophilic molecule, VAN, as shown in Figure 4e. Comparable loading value of 231.84 mg g⁻¹ and 237.52 mg g⁻¹ was achieved for MHS and RMHS respectively. However, the relatively hydrophobic nature of RMHS enabled sustained release behavior of VAN. RMHS releases 73% VAN at 6 h and 91% up to 36 h relative to 100% release achieved at 8 h for MHS (Figure 4f). RMHS is more hydrophobic compared to MHS; however it is still a pure silica material which cannot totally avoid the surface wetting especially in an aqueous solution (the drug release medium). The relatively higher energy barrier for wetting (or hydrophobicity) of RMHS over MHS is the underlying reason for the sustained drug release behavior.

The size of the core nanoparticles with similar morphology can be further finely tuned with the same preparation method. We have successfully prepared MHS and RMHS with an average core size of 200 and 13 nm shell particles size named as MHS200 and RMHS200. Both nanoparticles have similar surface morphology compared to the larger particles (MHS and RMHS) as shown by the TEM and SEM images in Figure S8. Their physiochemical properties are summarized in Table S1. MHS200 and RMHS200 have slightly smaller pore size (3.4 nm) and relatively higher pore volume (0.38 cm³ g⁻¹ for MHS200 and 0.62 cm³ g⁻¹ for RMHS200) compared to the larger sized particles. The mesopore volume (V_{meso}) is calculated to be 0.24 and 0.29 cm³ g⁻¹ for MHS200 and RMHS200, respectively.

The use of nanoparticles as a delivery vehicle for antibiotics provides a promising strategy through prolonged drug circulation half-life, increased availability of drugs interacting with membrane molecules, and promoted sustained drug release.³⁴ To compare the antibacterial performance of nanoparticles themselves and the influence of surface roughness, 4 groups of nanoparticles (MHS, RMHS, MHS200, RMHS200) were incubated with *Escherichia coli* (*E. coli*). The toxicity of the nanoparticles alone toward *E. coli* was evaluated by monitoring the optical density (OD) at 600 nm of a bacterial suspension (Figure S). It can be seen that all nanoparticles show dose-dependent antimicrobial performance. Moreover, at the same dose, the rough particles show lower OD₆₀₀ values (higher antimicrobial activity) compared to their smooth counterparts (RMHS vs MHS, and RMHS200 vs MHS200). This observation is more evident at high particle concentrations, suggesting improved interaction of nanoparticles with bacteria after introducing the surface roughness. In addition, RMHS200 with a size of 200 nm shows lower OD₆₀₀ values compared to RMHS with a larger particle size of ~400 nm consistently at all concentrations, indicating that smaller particles exhibit higher bacterial toxicity effect. This result is in accordance with a previous report showing the increasing of antibacterial activity with smaller particle size.³⁵

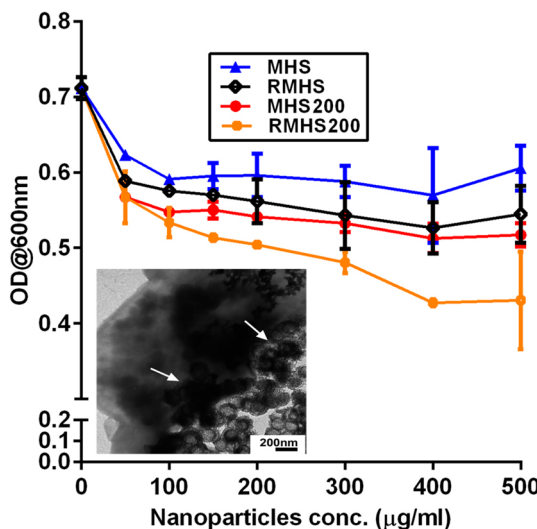


Figure 5. Concentration and size dependence on nanoparticles' toxicity of *E. coli* cultured for 24 h in LB media. Inset showing TEM image of RMHS200 in contact with the microbial surface giving toxicity to the microorganism.

Inset image showing assembled of RMHS200 nanoparticles on the microbial membrane giving toxicity and led to the death of the bacteria.

Because nanoparticles with smaller particle sizes have higher bacterial toxicity effect, MHS200 and RMHS200 were chosen as the VAN carriers for antimicrobial tests. VAN is a well-known glycopeptide antibiotic useful for the treatment of a number of bacterial infections since it inhibits the cell wall synthesis in susceptible bacteria.^{36–38} It is reported that VAN exhibits time-dependent bactericidal action and has little relation to drug concentrations.^{39,40} The *in vitro* antibacterial activity of free VAN, MHS200-VAN, and RMHS200-VAN was evaluated by the OD₆₀₀ measurement. *E. coli* (1×10^6 CFU mL⁻¹) was incubated in Luria–Bertani (LB) medium in a 1.5 mL centrifuge tube at various concentrations of VAN for 18 h. The minimum inhibitory concentration (MIC) value of free VAN toward *E. coli* was observed at 25 μg mL⁻¹ (Figure 6a). This value reduced to 16 μg mL⁻¹ for RMHS200-VAN, which is lower than the dosage used with VAN conjugated MCM-41 (200 μg mL⁻¹) in *in vitro* *E. coli* culture at 18 h.⁴¹ The MIC of MHS200-VAN is 20 μg mL⁻¹, larger than that of RMHS200-VAN but still lower than free VAN, showing improved antimicrobial activity of VAN delivered by nanocarriers, especially with the rough morphology. Loading of VAN in porous structure may preserve their activity compared to when immobilized on the surface of nanoparticles as the active site of VAN may be blocked.⁴²

In a separate experiment, MHS200-VAN, RMHS200-VAN, and free VAN with the same VAN content of 25 μg mL⁻¹ were incubated with 1×10^6 CFU mL⁻¹ *E. coli* in LB media and OD was measured as a function of time. It was observed that RMHS200-VAN inhibited the growth of bacteria faster (at 4 h) and maintained 100% inhibition throughout 24 h at the selected dosage. However, regrowth of bacteria as evidenced by increases in OD₆₀₀ was observed in both MHS200-VAN and free VAN groups after 18 h (Figure 6b). It was reported that the regrowth of bacteria exposed to VAN may occur if inadequately inhibited bacteria synthesize new peptidylglycan to override the antibacterial effect of VAN.⁴³ The 100% inhibition

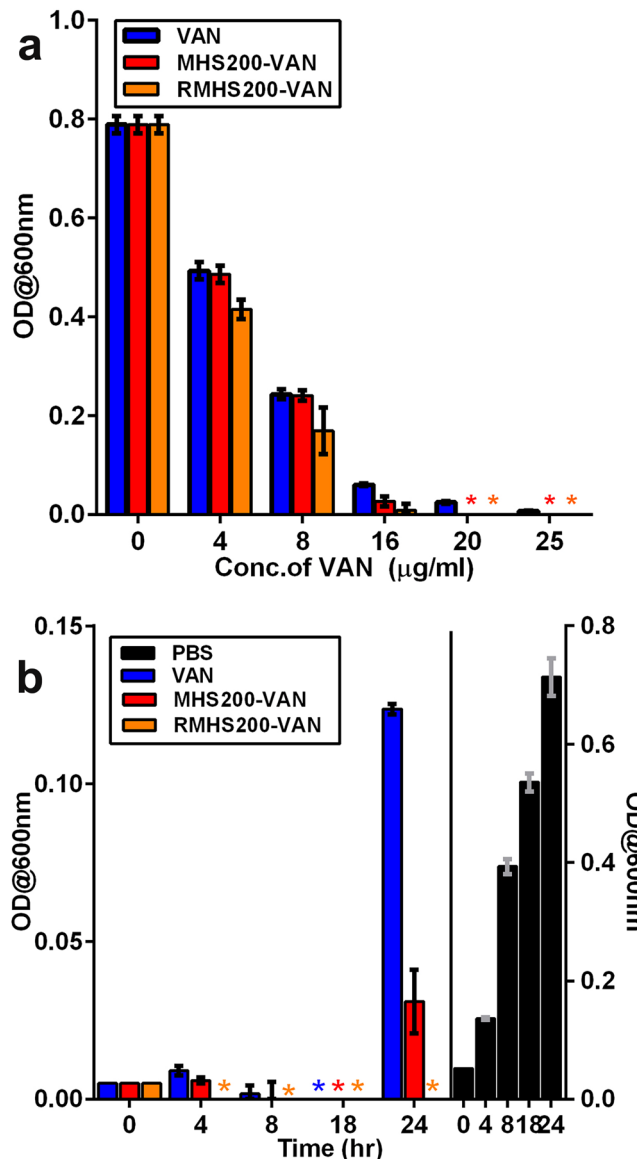


Figure 6. Antibacterial performance. (a) Dose-dependent antibacterial activity against *E. coli* of RMHS200-VAN, MHS200-VAN, and free VAN cultured for 18 h. (b) Time-dependent antibacterial study at the VAN dosage of 25 μg mL⁻¹ up to 24 h using PBS as a control. *indicated 100% inhibition. The error bars reflect the standard deviation of the measurements.

of *E. coli* even at 24 h in the case of RMHS200-VAN should be attributed to two advantages coming from the nanoparticle design: (1) the rough particles have a higher antimicrobial activity compared to their smooth counterparts (Figure 5); and (2) the more hydrophobic nature of RMHS200 associated with the higher wetting energy barrier compared to MSH200 leads to a sustained release of VAN compared to MHS200 (Figure S9), similar to the larger sized nanoparticles (Figure 4f). Collectively, RMHS200-VAN showed the lowest MIC value as measured at 18 h (Figure 6a), and the effective time window of the drug is increased to 24 h (Figure 6b).

To provide direct evidence on the antibacterial efficacy of nanoparticles, TEM was employed to observe the morphology of *E. coli* cultured at 24 h (Figure S10). For the untreated group (Figure S10a), the typical cylindrical morphologies of *E. coli* remained intact. Compared to the untreated group, VAN-

treated bacteria showed damage of the bacterial membrane (**Figure S10b–d**) with severe injuries of the wall/membrane of *E. coli* treated with RMHS-VAN (**Figure S10d**) was clearly observed. The cell cytotoxicity of MHS200 and RMHS200 in a normal cell line, human dermal fibroblast (HDF), was also assessed by the MTT assay. No significant cytotoxicity (less than 20%) of both nanoparticles even at a concentration of up to $500 \mu\text{g mL}^{-1}$ was observed (**Figure S11**), providing evidence of excellent bioinertness and safety of the materials as the carrier system. TEM image of the rough nanoparticles after pretreatment by sonication and further shaking in PBS (**Figure S12a**) as well as the TEM image of the particles under vigorous stirring (**Figure S12b**) for 36 h was also observed. The rough morphology is retained with no significant changes compared to the as-synthesized sample, suggesting that the hydrophobic property remains to play a role on the nanoparticles performance.

CONCLUSIONS

In summary, we have successfully prepared novel nanoparticles with a hydrophilic silica composition but having improved hydrophobic properties through surface roughness modification, which show higher loading capacity of hydrophobic molecules and sustained release for hydrophilic drugs compared to their counterparts with a smooth surface. The unique property of the nanoparticle's design affects their behavior in aquatic environment and influence the transport of the nanoparticles to the bacteria. The fundamental understanding gained from this study provides a new strategy for the development of nanocarriers with safe composition and high performance in widespread drug delivery applications.

ASSOCIATED CONTENT

Supporting Information

The Supporting Information is available free of charge on the ACS Publications website at DOI: [10.1021/acscentsci.5b00199](https://doi.org/10.1021/acscentsci.5b00199).

Methods for preparation of nanoparticles and supplemental data as noted in the text ([PDF](#))

AUTHOR INFORMATION

Corresponding Author

*E-mail: c.yu@uq.edu.au.

Notes

The authors declare no competing financial interest.

ACKNOWLEDGMENTS

The authors acknowledge the financial support from the Australian Research Council, the Queensland Government, the Australian National Fabrication Facility, and the Australian Microscopy and Microanalysis Research Facility at the Centre for Microscopy and Microanalysis, The University of Queensland.

REFERENCES

- (1) Cedervall, T.; Lynch, I.; Lindman, S.; Berggard, T.; Thulin, E.; Nilsson, H.; Dawson, K. A.; Linse, S. Understanding the nanoparticle-protein corona using methods to quantify exchange rates and affinities of proteins for nanoparticles. *Proc. Natl. Acad. Sci. U. S. A.* **2007**, *104*, 2050–2055.
- (2) Nel, A. E.; Mädler, L.; Velegol, D.; Xia, T.; Hoek, E. M. V.; Somasundaran, P.; Klaessig, F.; Castranova, V.; Thompson, M. Understanding biophysicochemical interactions at the nano–bio interface. *Nat. Mater.* **2009**, *8*, 543–557.
- (3) Xu, L. C.; Siedlecki, C. A. Effects of surface wettability and contact time on protein adhesion to biomaterial surfaces. *Biomaterials* **2007**, *28*, 3273–3283.
- (4) Salerno, M. B.; Logan, B. E.; Velegol, D. Importance of molecular details in predicting bacterial adhesion to hydrophobic surfaces. *Langmuir* **2004**, *20*, 10625–10629.
- (5) Yohe, S. T.; Colson, Y. L.; Grinstaff, M. W. Superhydrophobic materials for tunable drug release: using displacement of air to control delivery rates. *J. Am. Chem. Soc.* **2012**, *134*, 2016–2019.
- (6) Prakash, S.; Malhotra, M.; Shao, W.; Tomaro-Duchesneau, C.; Abbasi, S. Polymeric nanohybrids and functionalized carbon nanotubes as drug delivery carriers for cancer therapy. *Adv. Drug Delivery Rev.* **2011**, *63*, 1340–1351.
- (7) Sethuraman, A.; Han, M.; Kane, R. S.; Belfort, G. Effect of surface wettability on the adhesion of proteins. *Langmuir* **2004**, *20*, 7779–7788.
- (8) Rasch, M. R.; Rossinyol, E.; Hueso, J. L.; Goodfellow, B. W.; Arbiol, J.; Korgel, B. A. Hydrophobic gold nanoparticle self-assembly with phosphatidylcholine lipid: membrane-loaded and janus vesicles. *Nano Lett.* **2010**, *10*, 3733–3737.
- (9) Bale, S. S.; Kwon, S. J.; Shah, D. A.; Banerjee, A.; Dordick, J. S.; Kane, R. S. Nanoparticle-mediated cytoplasmic delivery of proteins to target cellular machinery. *ACS Nano* **2010**, *4*, 1493–1500.
- (10) Zhang, J.; Karmakar, S.; Yu, M. H.; Mitter, N.; Zou, J.; Yu, C. Z. Synthesis of silica vesicles with controlled entrance size for high loading, sustained release, and cellular delivery of therapeutic proteins. *Small* **2014**, *10*, 5068–5076.
- (11) Wu, S. H.; Mou, C. Y.; Lin, H. P. Synthesis of mesoporous silica nanoparticles. *Chem. Soc. Rev.* **2013**, *42*, 3862–3875.
- (12) Doadrio, J. C.; Sousa, E. M. B.; Izquierdo-Barba, I.; Doadrio, A. L.; Perez-Pariente, J.; Vallet-Regi, M. Functionalization of mesoporous materials with long alkyl chains as a strategy for controlling drug delivery pattern. *J. Mater. Chem.* **2006**, *16*, 462–466.
- (13) Xia, F.; Jiang, L. Bio-inspired, smart, multiscale interfacial materials. *Adv. Mater.* **2008**, *20*, 2842–2858.
- (14) Feng, L.; Li, S. H.; Li, Y. S.; Li, H. J.; Zhang, L. J.; Zhai, J.; Song, Y. L.; Liu, B. Q.; Jiang, L.; Zhu, D. B. Super-hydrophobic surfaces: From natural to artificial. *Adv. Mater.* **2002**, *14*, 1857–1860.
- (15) Feng, L.; Song, Y. L.; Zhai, J.; Liu, B. Q.; Xu, J.; Jiang, L.; Zhu, D. B. Creation of a superhydrophobic surface from an amphiphilic polymer. *Angew. Chem., Int. Ed.* **2003**, *42*, 800–802.
- (16) Erbil, H. Y.; Demirel, A. L.; Avci, Y.; Mert, O. Transformation of a simple plastic into a superhydrophobic surface. *Science* **2003**, *299*, 1377–1380.
- (17) Guo, Z. G.; Zhou, F.; Hao, J. C.; Liu, W. M. Stable biomimetic super-hydrophobic engineering materials. *J. Am. Chem. Soc.* **2005**, *127*, 15670–15671.
- (18) Bocquet, L.; Lauga, E. A smooth future? *Nat. Mater.* **2011**, *10*, 334–337.
- (19) Patankar, N. A. Transition between superhydrophobic states on rough surfaces. *Langmuir* **2004**, *20*, 7097–7102.
- (20) Ran, C. B.; Ding, G. Q.; Liu, W. C.; Deng, Y.; Hou, W. T. Wetting on nanoporous alumina surface: Transition between Wenzel and Cassie states controlled by surface structure. *Langmuir* **2008**, *24*, 9952–9955.
- (21) Adera, S.; Raj, R.; Enright, R.; Wang, E. N. Non-wetting droplets on hot superhydrophilic surfaces. *Nat. Commun.* **2013**, *4*, 1–7.
- (22) Guo, C. W.; Feng, L.; Zhai, J.; Wang, G. J.; Song, Y. L.; Jiang, L.; Zhu, D. B. Large-area fabrication of a nanostructure-induced hydrophobic surface from a hydrophilic polymer. *ChemPhysChem* **2004**, *5*, 750–753.
- (23) Weeks, J. D. Connecting local structure to interface formation: A molecular scale van der Waals theory of nonuniform liquids. *Annu. Rev. Phys. Chem.* **2002**, *53*, 533–562.
- (24) Chen, Y.; Chu, C.; Zhou, Y. C.; Ru, Y. F.; Chen, H. R.; Chen, F.; He, Q. J.; Zhang, Y. L.; Zhang, L. L.; Shi, J. L. Reversible pore-structure evolution in hollow silica nanocapsules: large pores for

siRNA delivery and nanoparticle collecting. *Small* **2011**, *7*, 2935–2944.

(25) Paunov, V. N. Novel method for determining the three-phase contact angle of colloid particles adsorbed at air-water and oil-water interfaces. *Langmuir* **2003**, *19*, 7970–7976.

(26) Cayre, O. J.; Paunov, V. N. Contact angles of colloid silica and gold particles at air-water and oil-water interfaces determined with the gel trapping technique. *Langmuir* **2004**, *20*, 9594–9599.

(27) Paunov, V. N.; Cayre, O. J. Supraparticles and "Janus" particles fabricated by replication of particle monolayers at liquid surfaces using a gel trapping technique. *Adv. Mater.* **2004**, *16*, 788–791.

(28) Arnaudov, L. N.; Cayre, O. J.; Stuart, M. A. C.; Stoyanov, S. D.; Paunov, V. N. Measuring the three-phase contact angle of nanoparticles at fluid interfaces. *Phys. Chem. Chem. Phys.* **2010**, *12*, 328–331.

(29) Xiao, Y.; Wiesner, M. R. Characterization of surface hydrophobicity of engineered nanoparticles. *J. Hazard. Mater.* **2012**, *215*–216, 146–151.

(30) Valle, R. P.; Huang, C. L.; Loo, J. S. C.; Zuo, Y. Y. Increasing hydrophobicity of nanoparticles intensifies lung surfactant film inhibition and particle retention. *ACS Sustainable Chem. Eng.* **2014**, *2*, 1574–1580.

(31) Lei, C.; Noonan, O.; Jambhrunkar, S.; Qian, K.; Xu, C.; Zhang, J.; Nouwens, A.; Yu, C. Z. Sensitive detection of human insulin using a designed combined pore approach. *Small* **2014**, *10*, 2413–2418.

(32) Ostuni, E.; Grzybowski, B. A.; Mrksich, M.; Roberts, C. S.; Whitesides, G. M. Adsorption of proteins to hydrophobic sites on mixed self-assembled monolayers. *Langmuir* **2003**, *19*, 1861–1872.

(33) Hudson, S.; Cooney, J.; Magner, E. Proteins in mesoporous silicates. *Angew. Chem., Int. Ed.* **2008**, *47*, 8582–8594.

(34) Zhang, L.; Pornpattananangkul, D.; Hu, C. M. J.; Huang, C. M. Development of nanoparticles for antimicrobial drug delivery. *Curr. Med. Chem.* **2010**, *17*, 585–594.

(35) Lemire, J. A.; Harrison, J. J.; Turner, R. J. Antimicrobial activity of metals: mechanisms, molecular targets and applications. *Nat. Rev. Microbiol.* **2013**, *11*, 371–384.

(36) Levison, M. E.; Levison, J. H. Pharmacokinetics and pharmacodynamics of antibacterial agents. *Infect. Dis. Clin. N. Am.* **2009**, *23*, 791–815.

(37) Sun, J. C.; Li, J. J.; Fan, H.; Ai, S. Y. Ag nanoparticles and vancomycin comodified layered double hydroxides for simultaneous capture and disinfection of bacteria. *J. Mater. Chem. B* **2013**, *1*, 5436–5442.

(38) Kell, A. J.; Stewart, G.; Ryan, S.; Peytavi, R.; Boissinot, M.; Huletsky, A.; Bergeron, M. G.; Simard, B. Vancomycin-modified nanoparticles for efficient targeting and preconcentration of Gram-positive and Gram-negative bacteria. *ACS Nano* **2008**, *2*, 1777–1788.

(39) Kohanski, M. A.; Dwyer, D. J.; Collins, J. J. How antibiotics kill bacteria: from targets to networks. *Nat. Rev. Microbiol.* **2010**, *8*, 423–435.

(40) Levison, M. E. Pharmacodynamics of antimicrobial drugs. *Infect. Dis. Clin. N. Am.* **2004**, *18*, 451–465.

(41) Qi, G. B.; Li, L. L.; Yu, F. Q.; Wang, H. Vancomycin-modified mesoporous silica nanoparticles for selective recognition and killing of pathogenic gram-positive bacteria over macrophage-like cells. *ACS Appl. Mater. Interfaces* **2013**, *5*, 10874–10881.

(42) Lai, H. Z.; Chen, W. Y.; Wu, C. Y.; Chen, Y. C. Potent antibacterial nanoparticles for pathogenic bacteria. *ACS Appl. Mater. Interfaces* **2015**, *7*, 2046–2054.

(43) Lowdin, E.; Odenholt, I.; Cars, O. In vitro studies of pharmacodynamic properties of vancomycin against *Staphylococcus aureus* and *Staphylococcus epidermidis*. *Antimicrob. Agents Ch.* **1998**, *42*, 2739–2744.